ARTICLES

Infrared spectroscopy investigation of the $CsHSeO_4$ superionic phase transition

D. De Sousa Meneses, P. Simon, and Y. Luspin
Centre de Recherche sur les Matériaux à Haute Température, CNRS, 45071 Orléans Cedex 2, France
(Received 5 March 1999)

The temperature dependence of the polarized infrared reflectivity spectra of cesium hydrogen selenate is reported between room temperature and 170 °C, and analyzed in the framework of the four-parameter model of the dielectric function. The results of the simulation show that the hydrogen-bond breaking starts far below T_C and the ratio η of protons involved in H-bond chains follows the law $\eta(T)=\exp[E/(T-T_0)]$ with $E=5.3$ K and $T_0=129$ °C. The protonic superionic phase transition is shown to occur at a topological threshold from a one-dimensional structure of H bonding to a structure of liquidlike nature. Such a microscopic mechanism, i.e., H-bond breaking, is consistent with previous results and explains the peculiar behavior of the elastic properties.

I. INTRODUCTION

Cesium hydrogen selenate $CsHSeO_4$ (hereafter denoted CHSe) is a solid electrolyte that exhibits a superionic protonic conduction behavior above $T_C=128$ °C.[1–4] The first-order phase transition is accompanied by a strong conductivity increase, by four orders of magnitude (up to $10^{-2}\,\Omega^{-1}\,\mathrm{cm}^{-1}$), which essentially originates from proton diffusion.[5–8] Furthermore, x-ray and optical studies have evidenced that the phase transition is of an improper ferroelastic type.[9–11] At room temperature, the crystal belongs to the monoclinic space group $P2_1/c(C_{2h}^5)$ with four formula units per unit cell and looks like a one-dimensional arrangement of H-bond chains along the *c* axis, with an O-H···O H-bond length of 2.6 Å (with the usual convention twofold axis along *b*).[12] Above T_C, the crystal structure is tetragonal and the space group is $I4_1/amd(D_{4h}^{19})$.[13,14] Besides this change of state, several experimental facts occurring below T_C (~ 80 °C) lead some authors to report the occurrence of another phase transition,[15–18] or to postulate that the structural phase transition in CHSe starts far below $T_C=128$ °C and thus that a two-phase region stands in the temperature range $80\rightarrow 128$ °C.[19] Other results[6,20] do not support such conclusions.

The same types of superionic behavior and phase transition sequence are also present in other crystals such as $CsHSO_4$ and deuterated analogs which are isomorphous to CHSe. Numerous papers on these compounds have been published for two decades (see Refs. 21–26 for the most recent ones), but as for CHSe there is no consensus on the phase transition sequence. Infrared spectroscopy gives access to all optic functions and is therefore a powerful tool to investigate changes of state such as ferroelectric or superionic phase transitions. Some infrared data of CHSe have been published recently,[16,27,28] but they are essentially absorptivity measurements made at room temperature. In the present paper, the temperature dependence of the reflectivity spectra of CHSe is reported from room temperature up to 170 °C for two polarizations of the incident beam. The results stemming from the simulation of the data shed new light on the superionic phase transition mechanism and lead to the characterization of hydrogen bonding.

II. EXPERIMENTAL PROCEDURE

Single crystals of CHSe were grown from saturated aqueous solutions by slow cooling from 40 °C down to 30 °C. Two samples were used: *ac* and *bc* platelets about $10\times 10\times 1$ mm^3 in size (obtained from a large single crystal), which were, respectively, used to acquire room-temperature reflectivity data for polarization along the *a* axis, and to obtain the temperature dependence of reflectivity spectra for polarizations of the electric field of the infrared electromagnetic wave along the *b* and *c* axes. The predominantly monodomain character of the single crystals can be checked with the room-temperature reflectivity data (Fig. 1) and the results of the fit (Table I) presented in the following. In each polarization there is a strong mode which is absent in both other polarizations, thus confirming the predominantly monodomain character of the single crystals and the predominant pure character of the eigenmodes. The infrared reflectivity spectra have been recorded under vacuum on a coupled Bruker IFS 113v-IFS 88 rapid-scan Fourier-transform interferometer, giving access to the spectral range 10–40 000 cm^{-1}. Only the 10–5000-cm^{-1} range relevant for the phase transition physics was recorded here. The spectra were recorded with an instrumental resolution of 4 cm^{-1}. The heating device was a hot plate, leading to temperature gradients in the sample lower than 1 °C.

III. ANALYSIS OF INFRARED REFLECTIVITY SPECTRA

A. Dielectric-function models

Infrared reflectivity spectroscopy provides, via Fresnel's relation near normal incidence, the complex dielectric function ε:

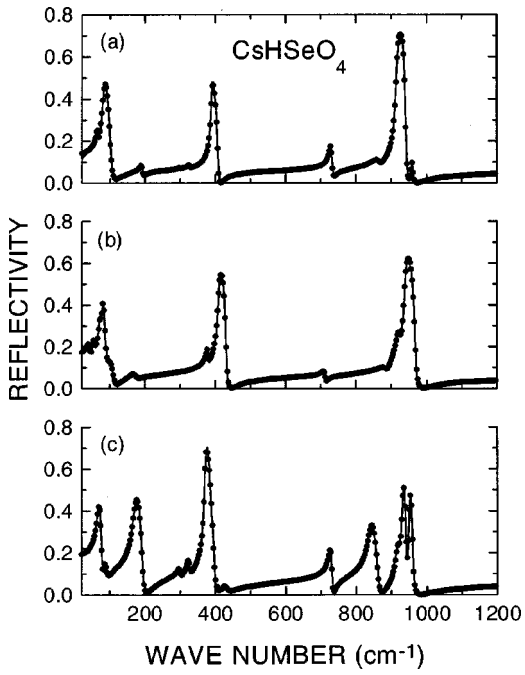

FIG. 1. Infrared reflectivity spectra of CsHSe for polarizations *a*, *b*, and *c* in the 20–1200-cm^{-1} spectral range. Full lines and dots, respectively, represent experiment and best fits performed with the factorized form of the dielectric function.

$$R=\left|\frac{\sqrt{\varepsilon}-1}{\sqrt{\varepsilon}+1}\right|^2, \tag{1}$$

where R is the reflectance. Theoretically it is possible to deduce the real and imaginary parts of the dielectric function through a Kramers-Krönig analysis of the reflection data. But this often leads to some uncertainties or mistakes due to the extension to zero and infinity of the low- and high-frequency edges of the experimental data, particularly when these edges are not flat. Another way recently developed is to use the maximum entropy method,[29–31] which does not require knowledge of the reflectivity spectra on the entire range of frequency but only needs the values of both and imaginary parts of the dielectric function for one or several frequencies situated in the measurement range. In this paper we use a model of the dielectric function and fit its adjustable parameters to the experimental reflectivity spectra through Fresnel's relation.

The factorized form, or four-parameter model,

$$\varepsilon(\omega)=\varepsilon_\infty\prod_j\frac{\Omega_{j\mathrm{LO}}^2-\omega^2+i\omega\gamma_{j\mathrm{LO}}}{\Omega_{j\mathrm{TO}}^2-\omega^2+i\omega\gamma_{j\mathrm{TO}}}, \tag{2}$$

was proposed by Kurosawa[32] and works well in numerous cases, including strongly damped soft modes.[33] In this model, each optical mode j [transverse optical (TO) or longitudinal optical (LO)] is described by two parameters, frequency Ω_j and damping γ_j. The TO modes are the complex poles of ε while the structure of LO modes is given by the imaginary part of $1/\varepsilon$. This model is an extension to finite frequencies of the Lyddane-Sachs-Teller relation. From the whole set of TO and LO frequencies, one can calculate the dielectric strength of each mode (often also called the oscillator strength)

$$\Delta\varepsilon_j=\varepsilon_\infty\Omega_{j\mathrm{TO}}^{-2}\frac{\Pi_k(\Omega_{k\mathrm{LO}}^2-\Omega_{j\mathrm{TO}}^2)}{\Pi_{k\neq j}(\Omega_{k\mathrm{TO}}^2-\Omega_{j\mathrm{TO}}^2)}, \tag{3}$$

and the static dielectric constant ε_0 (assuming there is no dispersion below the infrared spectral range)

$$\varepsilon(\omega=0)=\varepsilon_0=\varepsilon_\infty+\sum_j\Delta\varepsilon_j. \tag{4}$$

B. Symmetry of the vibration modes

In the room-temperature monoclinic phase, CHSe contains four formula units per primitive cell, leading to 84 modes. All ions ($HSeO_4^-$ and Cs^+) occupy general C_1 positions. Table I shows how the external modes, internal tetrahedron modes, and proton vibrations in the hydrogen bonds transform among the irreducible representations of the space group. The same analysis for the tetragonal phase is not made because of the quasiliquid nature of the high-temperature state. Indeed, the loss of translational symmetry due to proton diffusion and the fact that the tetragonal symmetry is only an average symmetry (almost free rotation of the selenate tetrahedron) preclude a rigorous analysis of the infrared activity in this phase.

IV. RESULTS AND DISCUSSION

A. Infrared spectra at room temperature

The infrared spectra of CHSe for polarization of the incident electromagnetic wave along *a*, *b*, and *c* are displayed in Figs. 1 and 2. The corresponding transverse- and longitudinal-optical frequencies obtained with the four-parameter model and mode assignments are summarized in

TABLE I. Reduction into irreducible representations of the 84 modes of CsHSe in the low-temperature phase. The tetrahedron internal modes are indicated with Herzberg's notation. T_a, acoustic modes; T, translational modes; R, librational modes; ν_1,ν_2,ν_3,ν_4, Herzberg's notation of the internal modes of selenate tetrahedron; $\nu_{\mathrm{OH}},\delta_{\mathrm{OH}},\gamma_{\mathrm{OH}}$ hydrogen-bond modes.

C_{2h}	T_a	T	R	ν_1	ν_2	ν_3	ν_4	ν_{OH}	δ_{OH}	γ_{OH}	IR activity
A_g	0	6	3	1	2	3	3	1	1	1	
B_g	0	6	3	1	2	3	3	1	1	1	
A_u	1	5	3	1	2	3	3	1	1	1	T_z
B_u	2	4	3	1	2	3	3	1	1	1	T_x,T_y

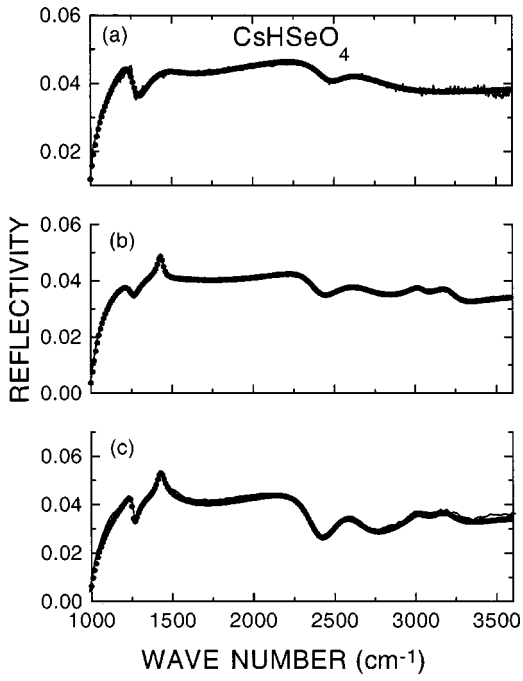

FIG. 2. Infrared reflectivity spectra of CsHSe for polarizations *a*, *b*, and *c* in the 1000–3500-cm^{-1} spectral range. Full lines and dots, respectively, represent experiment and best fits performed with the factorized form of the dielectric function.

Table II. The bands observed in the 250–4000 cm^{-1} range

TABLE II. Wave-number values (cm^{-1}) and the tentative assignment of all transverse- and longitudinal-optic frequencies of the modes used in the simulation of reflectivity spectra for polarizations *a*, *b*, and *c*.

Axis *a*		Axis *b*		Axis *c*		Tentative
Ω_{TO}	Ω_{LO}	Ω_{TO}	Ω_{LO}	Ω_{TO}	Ω_{LO}	assignment
		42.9	44.8			
		53.1	55.6			
64.6	65.4	71.1	74.1	67.4	79.1	Lattice modes
81.6	103.6	78.9	86.9	85.7	88.2	
		102.9	111.2	116.8	116.9	
		169.3	171.3	169.6	194.1	$\nu_{O\text{-}H\cdots O}$
298.0	298.1			299.3	300.6	$\nu_2 SeO_4$
325.9	326.2			324.7	326.6	$\nu_2 SeO_4$
389.9	408.1	377.6	378.9	370.7	386.8	$\nu_4 SeO_4$
404.3	397.5	409.1	431.6	426.4	429.7	$\nu_4 SeO_4$
728.6	733.3	711.7	713.5	725.9	732.7	$\nu_3 SeO_4$
				838.8	862.2	$\nu_1 SeO_4$
864.3	866.5	889.1	889.2	916.5	920.4	
914.8	941.1	919.2	923.1	930.5	941.0	$\nu_3 SeO_4$
956.7	960.6	937.1	967.1	947.7	959.4	$\nu_3 SeO_4$
1262.9	1269.6	1259.4	1260.3	1256.5	1258.4	δ_{OH}
		1431.7	1432.4	1427.1	1427.2	
1471.3	1482.7	1438.2	1487.5	1454.4	1487.4	$\nu_{OH}(C)$
2468.8	2469.4	2395.9	2404.5	2392.7	2404.6	$\nu_{OH}(B)$
2670.3	2719.75	2667.0	2688.1	2615.1	2650.3	$\nu_{OH}(A)$
		3030.5	3032.1	3028.5	3031.3	ν_{OH}
		3222.4	3227.4	3195.1	3199.4	ν_{OH}

arise from the internal modes of the selenate tetrahedron (250–1000 cm^{-1}), from the proton vibrations inside H bonds, and from overtones and combinations for high frequencies. The infrared bands observed below 250 cm^{-1} originate from lattice modes. These three spectral ranges will be discussed successively.

1. Internal vibrations of the selenate ions

Contrary to regular tetrahedra for which only ν_4 and ν_3 modes are infrared active, all the fundamental modes of the selenate ions appear in *c* polarization. The high intensity of ν_1 and ν_2 modes and the large splitting of ν_3 modes are consistent with the highly distorted structure of the tetrahedra. In the crystal the selenate ion has two short Se-O bonds (~1.6 Å), an intermediate bond (~1.62 Å), and a large bond of 1.71 Å.[13] Besides distortion, the existence of hydrogen chains along the *c* axis explains the great difference between *c* spectra and both the other two which look very similar. It can be assumed that the lowest ν_3 (730-cm^{-1}) mode is connected to the longest Se-O bond which is involved in the H-bond chain. The assignment of the ν_2 modes is supported by the fact that these modes lead to strong bands in Raman spectra. Similarly, the high intensity of the 838-cm^{-1} Raman mode and the value of the frequency of the totally symmetric ν_1 mode (837 cm^{-1}) in the free selenate ion lead us to think that the 838-cm^{-1} mode observed in the *c* polarization is also of ν_1 type.[17,27] The other bands in the 360–440-cm^{-1} and 700–1000-cm^{-1} ranges come, respectively, from the ν_4 and ν_3 selenate tetrahedron vibrations.

2. Hydrogen-bond vibrations

The out-of-plane γ (OH) bending mode seems to appear at 864 cm^{-1} in the spectrum polarized along the *a* axis and at higher frequencies in both other polarizations. These frequencies are slightly higher than those observed by inelastic neutron scattering (INS) and Raman techniques.[19,27] The in-plane δ (OH) bending mode lies at around 1260 cm^{-1} in all polarizations as in Raman spectra. The three bands at approximately 2650, 2400, and 1450 cm^{-1} are the so-called *ABC* bands which occur for particular conditions of H bonding.[34] These values are characteristic of medium H-bonding strength and are fully consistent with the 2.6-Å length of the O-H···O bonds in CHSe. Other bands are also present in this region; they are essentially overtones and combinations of two fundamental bands.

3. External vibrations

The low-frequency range 20–250 cm^{-1} corresponds to the translational and librational motion of the Cs^+ and $HSeO_4^-$ ions. A peculiar mode in this region, involving the H-bond chaining between tetrahedra, is the 169-cm^{-1} mode appearing predominantly in the *c* polarization. This mode $\nu_{O\text{-}H\cdots O}$ which is often observed in H-bond compounds arises from the stretching motion between SeO_3OH and $OSeO_3$ molecular ions.[17] It was denoted $\nu_{O\text{-}H\cdots O}$ in this reference and we will hereafter keep this notation, despite its somewhat ambiguous character: it is not a mode of individual O-H···O bonds.

B. Temperature dependence of the infrared spectra

Figures 3–6 display the temperature dependence of the infrared spectra of CHSe from room temperature up to

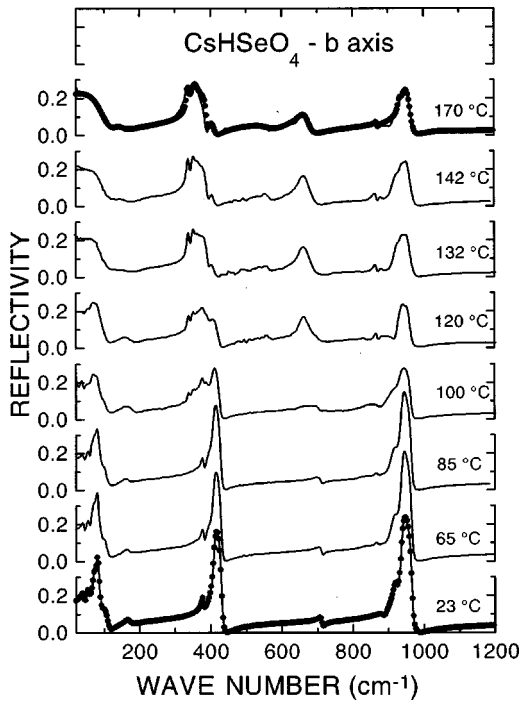

FIG. 3. Temperature dependence of the infrared reflectivity spectra of CsHSe in the 20–1200-cm^{-1} spectral range for the *b* polarization. Full lines and dots, respectively, represent experiments and best fits.

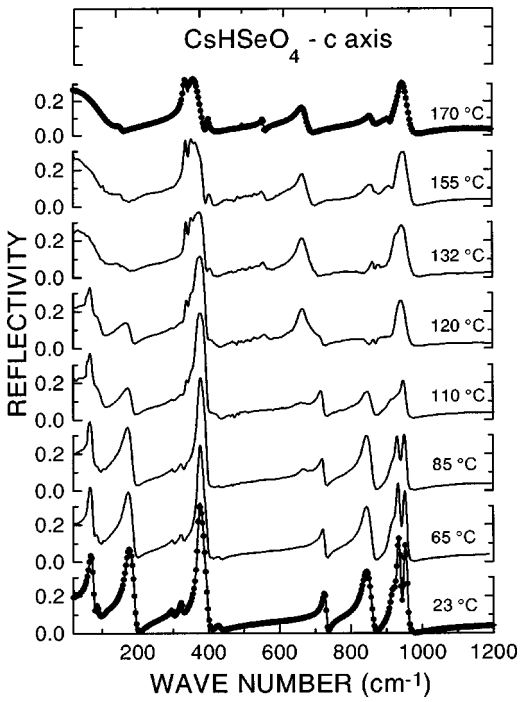

FIG. 5. Temperature dependence of the infrared reflectivity spectra of CsHSe in the 20–1200-cm^{-1} spectral range for the *c* polarization. Full lines and dots, respectively, represent experiments and best fits.

170 °C for polarization *b* and *c* of the electromagnetic IR wave. These two sets of curves respectively correspond to A_u and B_u irreducible representations of the low-temperature phase. Typical simulated curves obtained with the four-parameter model are also plotted. In the superionic phase, whatever the choice of model parameter values or oscillator number used in the ν_4 region, the fit always leads to negative values of the imaginary part of the dielectric function in the

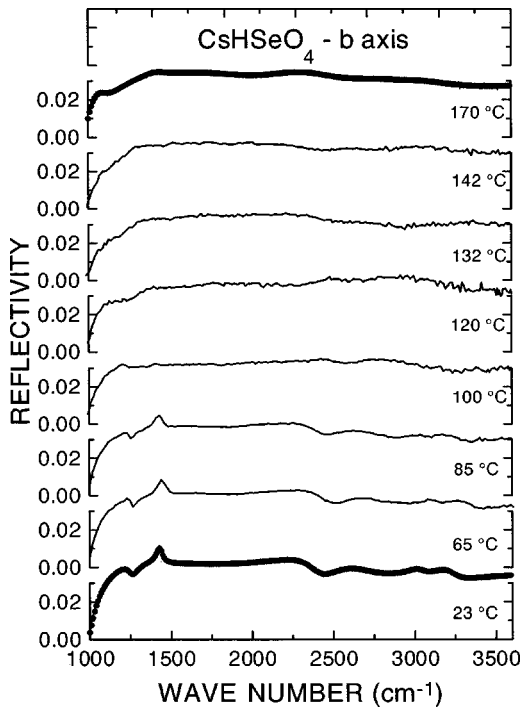

FIG. 4. Temperature dependence of the infrared reflectivity spectra of CsHSe in the 1000–3500-cm^{-1} spectral range for the *b* polarization. Full lines and dots, respectively, represent experiments and best fits.

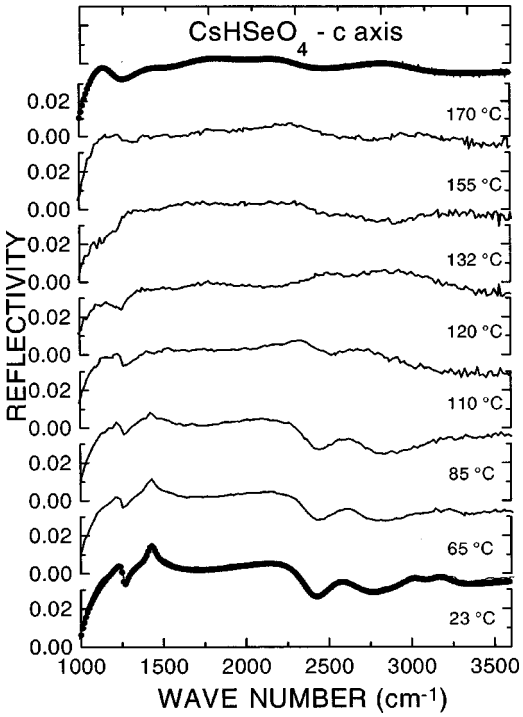

FIG. 6. Temperature dependence of the infrared reflectivity spectra of CsHSe in the 1000–3500-cm^{-1} spectral range for the *c* polarization. Full lines and dots, respectively, represent experiments and best fits.

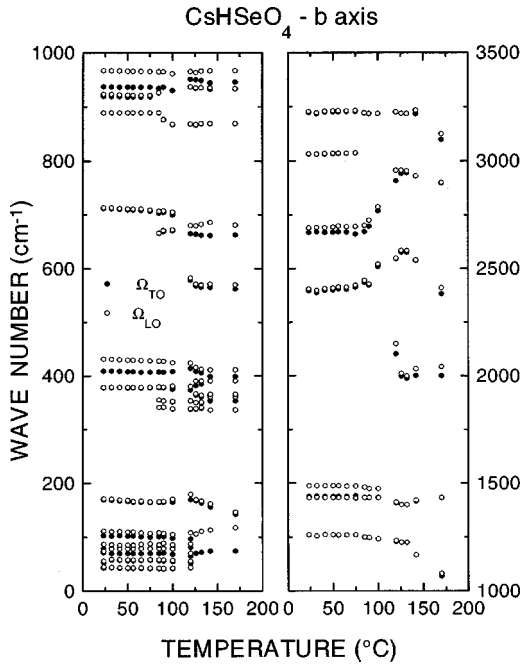

FIG. 7. Temperature dependence of the transverse- and longitudinal-optic frequencies of the oscillators used in the simulation of the infrared spectra of CsHSe for the *b* axis.

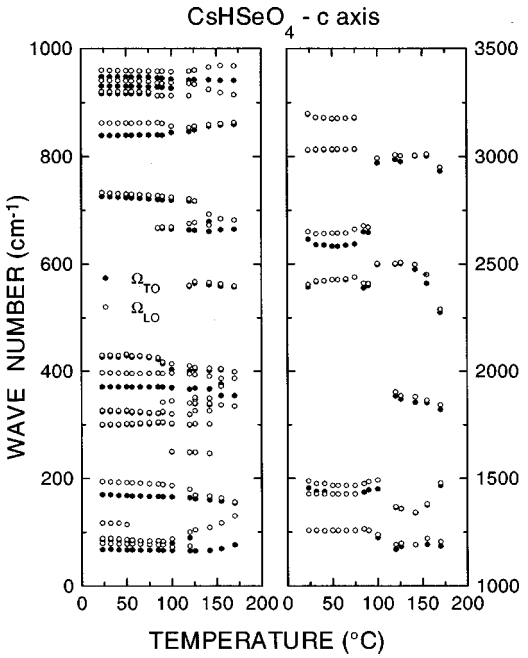

FIG. 8. Temperature dependence of the transverse- and longitudinal-optic frequencies of the oscillators used in the simulation of the infrared spectra of CsHSe for the *c* axis.

300–400-cm^{-1} range. This result that does not have any physical sense is due to the inability of the four-parameter model to describe such a profile of the ν_4 mode and more precisely to the abrupt form of the ν_4 low-frequency edge. The problem appears then due to a frequency dependence of damping stronger and more complex than the simple behavior with two values γ_{TO} and γ_{LO} assumed in the four-parameter model. The frequencies given by the fitting procedure are nevertheless quite correct. Fortunately, this problem is limited to this only spectral range and then it does not preclude a quantitative analysis of the temperature dependence of the parameters describing the dynamical behavior of CHSe. The temperature dependences of both longitudinal- and transverse-optic frequencies for all oscillators are displayed in Figs. 7 (polarization *b*) and 8 (polarization *c*). As can be seen in reflectivity measurements or in the oscillator parameter behavior, the onset of dynamical changes in CHSe starts far below T_C. Hence, these results confirm the experimental observation pointing out the occurrence of anomalies at approximately 80 °C. Nevertheless, it remains to answer the question: Is this intermediate regime a new phase (or the coexistence of two phases) in the thermodynamical sense? Before trying to answer, let us describe the main experimental results stemming from the simulation of the infrared data. The temperature range between 80 °C and T_C is characterized by the coexistence of the room-temperature modes and some modes of the superionic phase, such as modes of the ν_4 region and the mode at 670 cm^{-1} appearing in both the *b* and *c* spectra. Figure 9 displays the temperature dependence of the dielectric strength of some oscillators which are particularly sensitive to the approach of the change of state. Among these oscillators, those undergoing the more drastic changes are without doubt those of the *c* polarization, which are involved in the H-bond chains. The modes of the low-temperature phase behave in the same way, above 80 °C their dielectric strength abruptly falls until T_C. On the contrary, the emergent mode situated at 670 cm^{-1} behaves in the opposite way; this behavior is characteristic of an oscillator strength transfer between this mode and the 720-cm^{-1} mode. This result is consistent with the attribution of the 720-cm^{-1} mode to a stretching motion of the Se-OH mode involved in $(HSeO_4^-)_n$ chains. The 670-cm^{-1} mode is due to $(HSeO_4^-)_2$ dimers, the formation of which occurs when H-bond breaking (proton diffusion) appears.[35] The tempera-

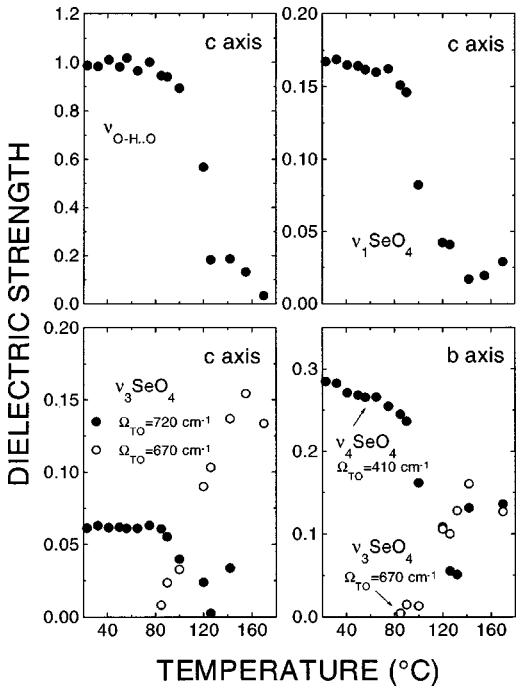

FIG. 9. Temperature dependence of the dielectric strength of several characteristic modes of CsHSe.

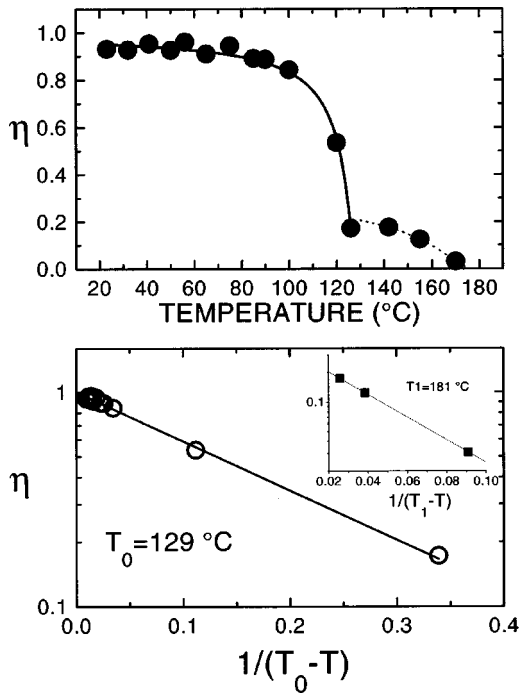

FIG. 10. Temperature dependence of the proton ratio involved in a hydrogen bond of the *c* chains. Full lines are best fits of the experimental data obtained with relation (5).

ture dependence of the $\nu_{\text{O-H}\cdots\text{O}}$ at 169 cm^{-1} is of particular interest. As its dielectric strength is proportional to the number of H bonds, this strength is a direct measurement of the ratio of protons which are effectively involved in the H bond chains along the *c* axis. The temperature dependence of this ratio η is displayed in Fig. 10; an excellent fit is obtained with a law

$$\eta(T)=\exp\left(\frac{E}{T-T_0}\right), \tag{5}$$

with the following parameters: $E=5.3\,\text{K}$ and $T_0=402\,\text{K}$ $\sim T_C$. In this law, T_0 is the temperature for which all the H bonds are broken. These results indicate that a dynamical disorder appears in CHSe above 80 °C, and that this disorder is essentially due to proton diffusion. The occurrence of disorder far below T_C is confirmed by the important broadening of the infrared lines. Examples of such a broadening are shown in Fig. 11. The damping curves obtained with the following law:

$$\gamma(T)=\gamma_0+\gamma_C[1-\eta(T)] \tag{6}$$

are well fitted with the parameters E and T_0 of the ratio η. These results confirm that the decrease of the $\nu_{\text{O-H}\cdots\text{O}}$ oscillator strength and the increase of damping are due to the same microscopic mechanism, i.e., H-bond breaking (proton diffusion). The very short characteristic time of infrared spectroscopy compared to those of relaxation processes inducing disorder leads to reflectivity spectra showing superposition of instantaneous pictures of the different microscopic configurations. Such an effect was already reported in other order-disorder transitions, as in sodium nitrite[36] where the lattice modes characteristic of the low-temperature phase are always observable more than 50 °C above T_C. We can

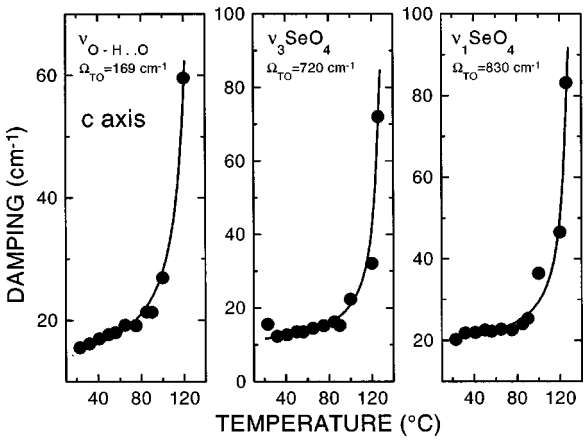

FIG. 11. Temperature dependence of the transverse damping of several modes of CsHSe. Full lines are best fits of the experimental data obtained with relation (6).

conclude, in the light of these results, that the intermediate regime between 80 °C and T_C is neither a new phase in the thermodynamical sense, nor a coexistence of two phases. This is consistent with the fact that authors using techniques with longer characteristic times do not see any anomaly in their measurements on freshly grown samples in this temperature range.

Let us now deal with the superionic phase transition. The appearance of the plastic phase at T_C is characterized by a drastic change in the region of external vibrations. Indeed, above T_C the low-temperature well-defined phonon structures give way to a single broad band in both orientations. The same behavior is seen in Raman spectra where the external bands collapse into a broad wing between 100 cm^{-1} and the Rayleigh line.[17] The INS spectra[19] also exhibit considerable changes and particularly a strong broadening of the peaks due to librations of the SeO_4 tetrahedrons. All these experimental results are direct proofs of the existence of a significant disorder of cations and anions in this phase, i.e., almost free rotation of the SeO_4 tetrahedrons and transla-

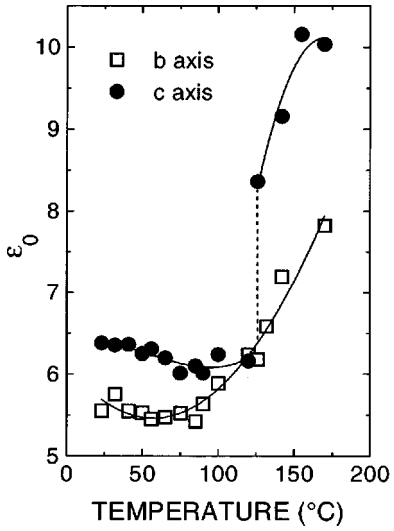

FIG. 12. Temperature dependence of the contribution of phonons to the static value of the dielectric function for the polarization *b* and *c*. Full lines are guides for the eyes.

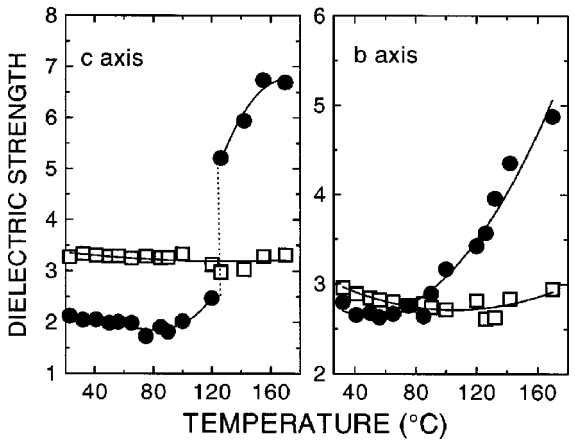

FIG. 13. Temperature dependencies of the contribution of the external modes (full circles) and internal modes (open squares) to the static value of the dielectric function for the polarization *b* and *c*. Full lines are guides for the eyes.

tional disorder of H^+ which are characteristic of the quasiliquid nature of the superionic conductor phase. Significant alterations of the H bonds also occur in the vicinity of the phase transition (Figs. 7 and 8). The so-called *ABC* bands located, respectively, at 2620, 2400, 1450 cm^{-1} in the low-temperature phase shift to approximately 3000, 2500, 1900 cm^{-1} above T_C. This can account for an increase of the averaged hydrogen length bonds of about 0.1 Å and is consistent with weaker hydrogen bonding.[34]

The temperature dependence of phonon contributions to the static dielectric constant along *b* and *c* axes is displayed in Fig. 12. The contribution along the *b* axis presents an important but continuous increase above 80 °C without peculiar behavior at the phase transition temperature. The *c*-polarization value behaves differently; it is relatively constant until T_C where it undergoes a large jump. Both types of temperature behaviors are essentially due to the external vibration modes (see Fig. 13) and are of course intimately connected with the one-dimensional arrangement of H bonds.

Along with the above discussion, there are several experimental evidences that the occurrence of the superionic state in CsHSe is a direct consequence of a thermally activated process that involves H-bond breaking in the proton chains. Nevertheless, it remains to explain why the phase transition only occurs when about (statistically speaking) 80% of the H bonds lying in the chains are broken; a value that is somewhat more constant than 10 K above T_C (Fig. 10). A possible explanation of this situation is of a topological nature. Indeed, if one looks at the CsHSe structure, one can see that each primitive cell contains four H bonds equally distributed in two chains (Fig. 14). To lose the one-dimensional arrangement of the H bonds on a large length scale, it is necessary to break at least three of the four H bonds in each primitive cell, and then the value of about 80% appears more as a topological or percolation threshold for which the one-dimensional structure of H bonds disappears at a large length scale. At T_C, the inability of the protons to maintain such a one-

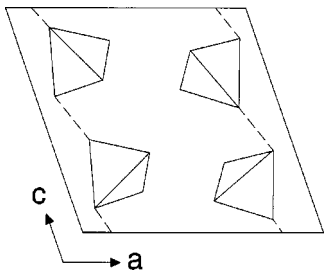

FIG. 14. Schematic representation of the primitive cell of CsHSe in the *ac* plane. Dashed lines represent hydrogen bonds.

dimensional arrangement leads to a more symmetric structure of a liquidlike nature that minimize the Gibbs free energy. Above T_C, the amount of protons that are still involved in a H bond follows a law analogous to relation (5), with an energy barrier parameter $E = 26.5$ K about five times higher than the value of the low-temperature phase and a temperature $T_1 = 454$ K (Fig. 10). This temperature is very close to that of a phase change which is somewhat universal in another class of hydrogen-bonded materials, KH_2PO_4-type compounds, and which is the most often interpreted in terms of the formation of one water molecule per unit formula from H bonds. Such a phase change was reported at least in KH_2PO_4, KD_2PO_4, RbH_2PO_4, $NH_4H_2PO_4$, and KH_2AsO_4,[37–39] and this temperature of 450 K can then be connected with an instability in the topology of the H-bond network.

Such a thermally activated process governed by topological constraints is consistent with the experimental results reported in the literature. Moreover, it is able to especially explain the very peculiar behavior of the elastic constants obtained by Brillouin-scattering measurements that were never explained satisfactorily until now. Indeed, the absence of pretransitional effects in the temperature dependence of the C_{11}, C_{22}, and C_{33} elastic constants[18] (normally expected in current phase transitions) can be explained by the fact that elastic constants are little influenced by H-bond changes which are the main modification that occurs in CsHSe below T_C. The strong discontinuities of the elastic constants appearing at T_C evidently result from the huge structural change taking place when the percentage of protons involved in a H-bond chain is lower than the percolation threshold for which a one-dimensional bond arrangement could stand.

V. CONCLUSION

From polarized reflectivity measurements obtained by infrared spectroscopy, the temperature behavior of hydrogen bonding has been determined. Results show that H-bond breaking is the key feature responsible for the occurrence of a protonic superionic state at high temperature. Breaking in the *c* chains starts far below T_C and the change of state occurs when the H-bond-breaking ratio reaches a topological threshold for which the one-dimensional hydrogen arrangement disappears. It will be interesting to check if such ideas developed for the understanding of the CsHSe phase transition also apply to the wide family of solid electrolytes that exhibit protonic superionic states.

[1] D. Foose and G. Mitra, J. Inorg. Nucl. Chem. **39**, 553 (1977).
[2] J. Wolak and Z. Czapla, Phys. Status Solidi A **67**, K171 (1981).
[3] S. Yokota, N. Takanohashi, T. Osaka, and Y. Makita, J. Phys. Soc. Jpn. **51**, 199 (1982).
[4] R. Blinc, J. Dolinsek, G. Lahajnar, I. Zupancic, L. A. Shuvalov, and A. I. Baranov, Phys. Status Solidi B **123**, K83 (1984).
[5] A. I. Baranov, L. A. Shuvalov, and N. M. Shchagina, Pis'ma Zh. Eksp. Teor. Fiz. **36**, 381 (1982) [JETP Lett. **36**, 459 (1982)].
[6] Y. N. Moskvich, A. M. Polyakov, and A. A. Sukhovkii, Fiz. Tverd. Tela (Leningrad) **30**, 40 (1988) [Sov. Phys. Solid State **30**, 24 (1988)].
[7] B. Hilczer, C. Pawlaczyk, and F. E. Salman, Ferroelectrics **81**, 193 (1988).
[8] Y. N. Moskvich, A. M. Polyakov, and A. A. Sukhovkii, Ferroelectrics **81**, 197 (1988).
[9] S. Yokota and Y. Makita, J. Phys. Soc. Jpn. **51**, 9 (1982).
[10] S. Yokota, J. Phys. Soc. Jpn. **51**, 1884 (1982).
[11] M. Komakue, M. Tanaka, T. Osaka, Y. Makita, K. Kozawa, and T. Uchida, Ferroelectrics **96**, 199 (1989).
[12] J. Baran and T. Lis, Acta Crystallogr., Sect. B: Struct. Sci. **43**, 811 (1986).
[13] M. Komukae, M. Tanaka, T. Osaka, Y. Makita, K. Kozawa, and T. Uchida, J. Phys. Soc. Jpn. **59**, 197 (1990).
[14] A. M. Balagurov, A. I. Beskrovnyi, I. D. Datt, L. A. Shuvalov, and N. M. Shchagina, Kristallografiya **31**, 1087 (1986) [Sov. Phys. Crystallogr. **31**, 643 (1986)].
[15] B. Baranowski, M. Friesel, and A. Lunden, Z. Naturforsch. Teil A **41**, 981 (1986).
[16] M. Pham-Thi, Ph. Colomban, A. Novak, and R. Blinc, Solid State Commun. **55**, 265 (1985).
[17] Ph. Colomban, M. Pham-Thi, and A. Novak, Solid State Ionics **20**, 125 (1986).
[18] Y. Luspin, Y. Vaills, and G. Hauret, Solid State Ionics **80**, 277 (1995).
[19] A. V. Belushkin, I. Natkaniec, N. M. Pakida, L. A. Shuvalov, and J. Wasicki, J. Phys. C **20**, 671 (1987).
[20] B. Kosturek and J. Przelawski, Ferroelectrics **80**, 273 (1988).
[21] B. Baranowski, J. Lipkowski, and A. Lundén, J. Solid State Chem. **117**, 412 (1995).
[22] A. V. Belushkin, M. A. Adams, S. Hull, A. I. Kolesnikov, and L. A. Shuvalov, Physica B **213&214**, 1034 (1995).
[23] N. Rangavittal, T. N. Guru Row, and C. N. R. Rao, J. Solid State Chem. **117**, 414 (1995).
[24] W. Münch, K. D. Kreuer, U. Traub, and J. Maier, J. Mol. Struct. **381**, 1 (1996).
[25] L. Kirpichnikova, M. Polomska, J. Wolak, and B. Hilczer, Solid State Ionics **97**, 135 (1997).
[26] A. Damyanovich, M. M. Pintar, R. Blinc, and J. Slak, Phys. Rev. B **56**, 7942 (1997).
[27] J. Baran, J. Mol. Struct. **162**, 229 (1987).
[28] H. Ratajczak, A. M. Yaremko, and J. Baran, J. Mol. Struct. **275**, 235 (1992).
[29] K.-E. Peiponen and E. M. Vartiainen, Phys. Rev. B **44**, 8301 (1991).
[30] E. M. Vartiainen, K.-E. Peiponen, and T. Asakura, Appl. Opt. **32**, 1126 (1993).
[31] E. M. Vartiainen, K.-E. Peiponen, and T. Asakura, Appl. Spectrosc. **50**, 1283 (1996).
[32] T. Kurosawa, J. Phys. Soc. Jpn. **16**, 1298 (1963).
[33] F. Gervais, in *Infrared and Millimeter Waves*, edited by K. J. Button (Academic, New York, 1983), Vol. 8, Chap. 7, p. 279.
[34] W. C. Hamilton and J. A. Ibers, *Hydrogen Bond in Solids* (Benjamin, Amsterdam, 1968).
[35] M. Gargouri, T. Mhiri, and A. Daoud, J. Phys.: Condens. Matter **9**, 10 977 (1997).
[36] F. Bréhat and B. Wyncke, J. Phys. C **18**, 1705 (1985).
[37] J. Grünberg, S. Levin, I. Pelah, and D. Gerlich, Phys. Status Solidi B **49**, 857 (1972).
[38] A. C. Pastor and R. C. Pastor, Ferroelectrics **71**, 61 (1987).
[39] B. M. Zhigarnovskii, Y. A. Polyakov, V. I. Bugakov, M. A. Maifat, K. Rakhimov, N. G. Moisashvili, O. G. Takaishvili, A. G. Mdinaradze, and V. P. Orlovskii, Inorg. Mater. (Transl. of Neorg. Mater.) **20**, 1074 (1984).